B. L. Josefson
Division of Solid Mechanics,
Chalmers University of Technology,
S-412 96, Göteborg, Sweden

L. O. Wikander
Division of Computer Aided Design,
Luleå University of Technology,
S-971 87 Luleå, Sweden

J. F. Hederstierna

F. K. Johansson

Division of Solid Mechanics,
Chalmers University of Technology,
Göteborg, Sweden

Welding Residual Distortions in Ring-Stiffened Pipes

A fast and simple method for the determination of the residual deformation for a class of welding problems, ring-stiffened pipes, is proposed. The method can predict radial as well as angular distortion of the thin-walled pipe-ring-stiffener/flange assembly. The pipe and stiffener material is elasto-plastic. In particular, the accumulation of deformation in multipass welding is incorporated in the model. Each weld pass is treated separately. This facilitates the assessment of the influence of the sequence in which the weld passes are deposited on the residual deformation state. The method will be included in a conversational knowledge-based "expert" system for the production of a welded ring-stiffened pipe.

Introduction

Today it is possible to perform detailed thermal and mechanical FE-analyses of a welding process in order to find both the transient and residual stress field present in the welded structure. Material nonlinearities caused by temperature dependence of material parameters and complex constitutive behavior of the weld pool and during final phase transformations can be accounted for; see the review by Goldak et al. (1992). Special FE-software for analysis of welding mechanics problems have been developed by several research groups.

However, detailed FE-analyses are time-consuming, even if computers with both high CPU and I/O-capacities are employed. In many cases, in particular when complex weldments, like multipass welds, are studied, one has to simplify the geometrical model or reduce the number of dimensions used (see, for example, Brown and Song, 1992); or simplify the thermal loading (see, for example, Bushnell, 1976; and Josefson, 1993).

Several expert systems have been developed the last years; see recent overviews by Barborak et al. (1991), Lucas (1994), and Cheng and Peng (1994). However, these systems focus primarily on metallurgical, production technology, weld cracking, or economical considerations. If one would also like to include information about the influence of the welding parameters and the geometry of structure and the groove on the residual deformation and stress field, it is necessary to reduce the time for the mechanical welding analysis, and thus to simplify the problem. This is particularly true when a conversational knowledge-based computer system shall be used.

Present Investigation

Such a simplified model is presented in this paper for the case of fillet welding of a ring to a thin-walled pipe. The objective is to estimate, by a rapid numerical analysis, the residual deformation of the welded structure. It is not intended to calculate, in detail, the transient or residual welding stress field. With the present approach, a qualitative and also quantitative picture of the buildup of the welding distortion during welding of a pipe-flange joint can be achieved using very few degrees of freedom and with a very small memory requirement. Compared to the pipe and ring stiffener models proposed by Moshaiov and Song (1990, 1991) and Song and Moshaiov (1990), where only the radial displacement w is used, our model includes also the cross-sectional rotation of the ring stiffener θ and the position of the weld passes.

Pipe-Ring Stiffener Model. The stiffened pipe is divided into three parts: two pipe parts (left l and right r) and the intermediate ring, including the part of the pipe located beneath the ring. This latter part is hereafter denoted as the ring stiffener. Each of the pipe parts are, in turn, divided into two parts: one two-node, elasto-plastic, finite element located closest to the ring, and one elastic shell of finite length. Both the structure and the thermal loading are considered to be rotationally symmetric. In our examples, the material in the pipe and ring stiffener is an austenitic stainless steel (Swedish standard SIS 142343) corresponding to grade 316. The deformation of the ring stiffener is controlled by two parameters: the radial displacement w and the rotation θ of the cross section for the ring stiffener. Figure 1 shows the geometry of the pipe-ring stiffener assembly. The pipe has the total length $L_{p,l} + L_{p,r} + w_r$ and the wall thickness t_p. The ring stiffener has the width w_r and the height h_r. The location of a typical weld pass is also indicated in Fig. 1. The weld pass is assumed to have a quadratic cross-sectional area $t_w \times t_w$, and its location is defined by the axial distance x_w and the radial distance y_w from the center of the area $t_w \times t_w$ to a reference point (RP) on the pipe outer surface at the distance $w_r/2$ from one of the vertical sides of the ring; see Fig. 1. One may note that with weld passes being successively added, the centroidal axis of the ring stiffener (CA) will move during the analysis. However, in our calculations, we have neglected this movement of CA and the corresponding changes in cross-sectional area and moment of inertia of the ring stiffener. Figure 2 shows the local degrees of freedom in the ring, shell elements, and the remote parts of the pipe, respectively. Figure 2 also shows the corresponding global degrees of freedom forming the condensed "displacement" vector $\{D\}$; (the axial displacement of the ring stiffener is put to zero to avoid rigid body displacements). Note that only two components of the calculated $\{D\}$—the transverse displacement (w or D_4) and cross-sectional rotation of the ring stiffener (θ or D_5) for the point CA in the ring stiffener (see Fig. 2)—will be presented in the Examples section.

Ring. The ring is assumed to have an undeformable cross section; thus, it will behave as a curved beam with an approximately uniaxial stress state. When the ring is elastic, formulas

Contributed by the OMAE Division and presented at the 14th International Symposium and Exhibit on Offshore Mechanics and Arctic Engineering, Copenhagen, Denmark, June 18–20, 1995, of THE AMERICAN SOCIETY OF MECHANICAL ENGINEERS. Manuscript received by the OMAE Division, July 26, 1995; revised manuscript received January 17, 1996. Associate Technical Editor: S. Liu.

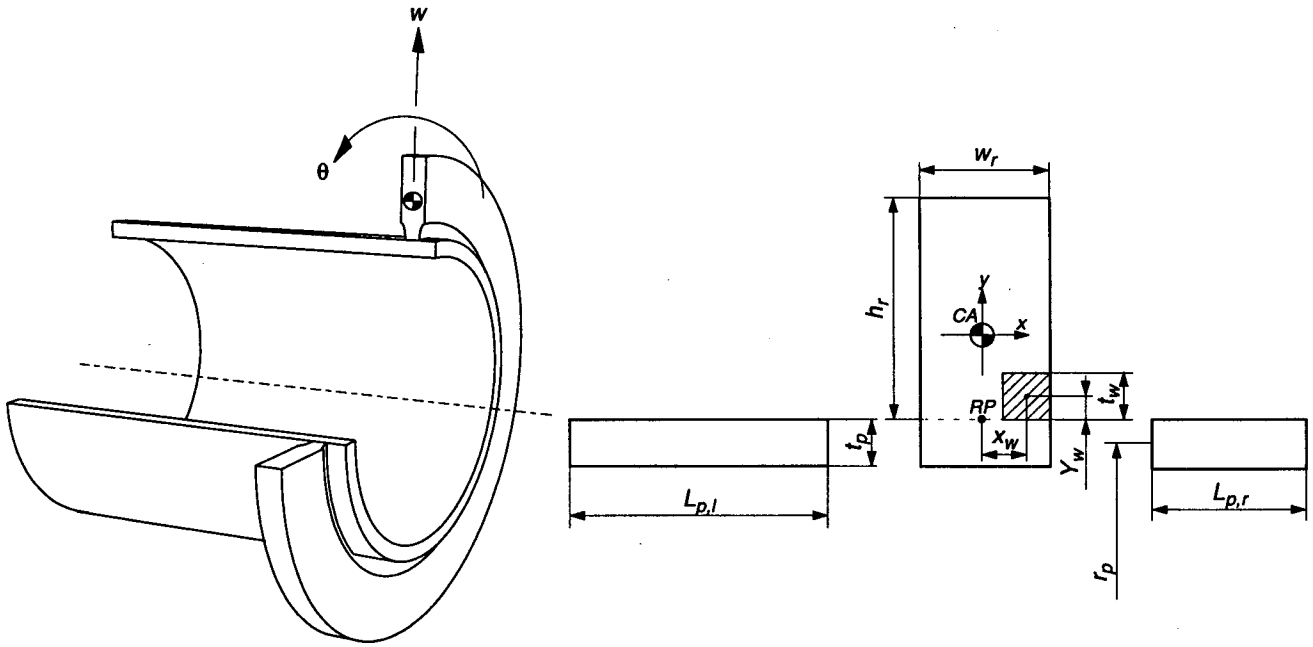

Fig. 1 Geometry of pipe-ring-stiffener assembly. Locations of weld passes are indicated.

from standard textbooks will apply. Due to the thermal load, a radial displacement w and rotation θ at the CA of the ring will develop, resulting in a hoop strain ϵ_ϕ, denoted ϵ. In a point at a distance x and y from CA, see Fig. 1, this strain will be

$$\epsilon = \frac{w + x\theta}{r + y} \tag{1}$$

where r is the radial distance from the axis of rotation to CA in the ring. This strain is decomposed into three different parts: the elastic part, the thermal part, and the plastic part. With Young's modulus E, the thermal strain ϵ^T taken as the linear thermal expansion coefficient times the temperature change, we obtain, formally, the hoop stress σ_ϕ, denoted σ, in weld metal from pass k at the end of a load step from time t to time $t + \Delta t$

$$\sigma_{t+\Delta t} = E(\epsilon_{t+\Delta t} - \epsilon^p_{t+\Delta t} - \epsilon^T_{t+\Delta t}) \tag{2}$$

The total contribution of shear force and bending moment from the ring, P_r and M_r, is obtained by integrating the hoop stress distribution, Eq. (2), over the cross-sectional area A of the ring

$$P_r = \frac{1}{r}\int_A \sigma dA \quad M_r = \frac{1}{r}\int_A x\sigma dA \tag{3}$$

The thermal strain associated with the welding of one layer of passes is large enough to create plastic deformation in the ring, ϵ^p in Eq. (2). The austenitic stainless steel used for the ring is assumed to have the virgin yield stress σ_Y (the same value in both tension and compression) and to follow Pragers kinematic hardening rule with a constant value for the hardening modulus H (and corresponding tangent modulus E_t). Note that the assumption on undeformable cross section contradicts the experimental finding that the plastic volume change is zero. We will, therefore, adopt the so-called simple kinematic hardening rule; see, for example, Cook et al. (1989).

Thus, we obtain the yield function, F, the plastic strain increment, ϵ^p, and the translation of the center of the yield curve, $\Delta\alpha$, as

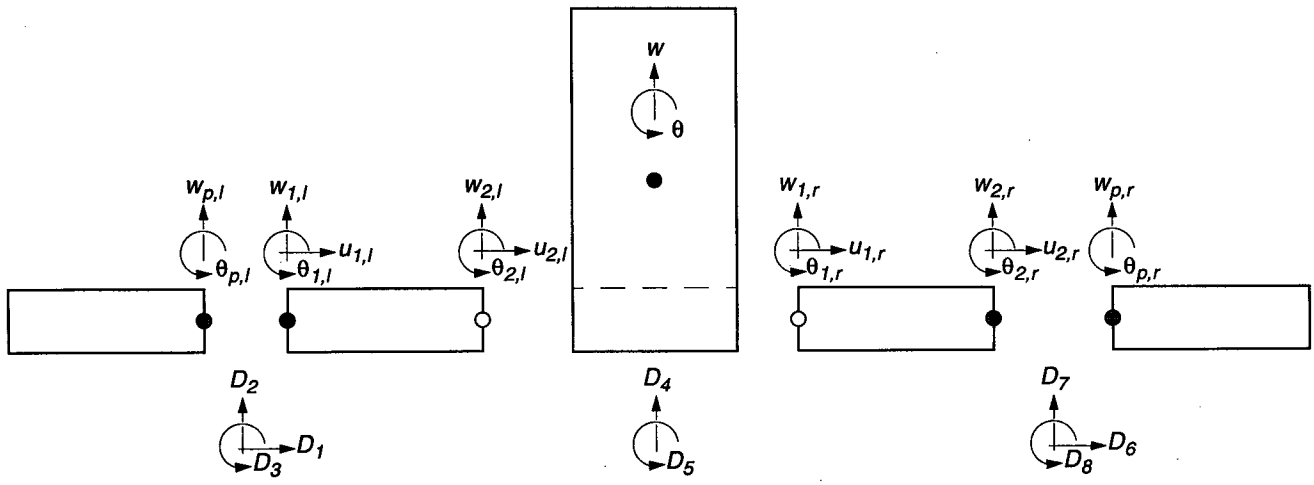

Fig. 2 Local degrees-of-freedom for the ring stiffener, the shell elements, and remote parts of the pipe. Below the ring stiffener, components of the condensed global displacement vector {*D*} for assembled structure are shown.

$$F = |\sigma - \alpha| - \sigma_y \quad \Delta\epsilon^p = \Delta\lambda \frac{\partial F}{\partial \sigma} = \frac{\Delta\sigma}{H}$$

$$\Delta\alpha = H\Delta\epsilon^p = \Delta\sigma \tag{4}$$

Remote Part of Pipe. The remote part of both pipe halves are assumed to be thin-walled and have a finite length. Furthermore, they are assumed to be elastic, and to be at room temperature, during the complete welding process. Standard textbooks in strength of materials will provide the stiffness for edge-loaded thin-walled elastic pipes; that is, the relation between sectional forces, the shear force P, and the bending moment M, at the interface between this part of the pipe and the shell finite elements and the nodal degrees of freedom, $\{d_{p,l}\} = [w_{p,l}\theta_{p,l}]^T$ and $\{d_{p,r}\} = [w_{p,r}\theta_{p,r}]^T$, respectively, see Fig. 2.

Shell Finite Element. The pipe part on each side of the ring stiffener located near the ring stiffener is modeled as a two-node rotationally symmetric shell element (Tessler, 1982). This element employs Mindlin plate theory; thus, transverse shear is included in the analysis. It has a linear axial variation of the axial displacement and cross-sectional rotation and a quadratic transverse displacement variation in the axial direction. To model possible plastic deformations in the pipe (close to the stiffener), the effective-stress-function approach (Kojic and Bathe, 1987) has been incorporated into the two-node shell element to calculate the proper stress state for a given strain state when the material becomes elasto-plastic.

The nodal degrees of freedom at the end of the shell finite elements facing the ring stiffener must be transformed to the centroidal axis (CA) of the ring. As noted in the foregoing, the ring stiffener is assumed to have an undeformable cross section. Using standard formulas for a "rigid link" in FE-codes (see, for example, Cook et al., 1989), one obtains the transformed element displacement vector $\{d_{sh}\}$ for the shell elements. For the left shell element, one has, for example,

$$\{d_{sh,l}\} = \begin{bmatrix} 1 & 0 & 0 & 0 & 0 & 0 \\ 0 & 1 & 0 & 0 & 0 & 0 \\ 0 & 0 & 1 & 0 & 0 & 0 \\ 0 & 0 & 0 & 1 & 0 & \frac{h_{rs}}{2} \\ 0 & 0 & 0 & 0 & 1 & \frac{-w_{rs}}{2} \\ 0 & 0 & 0 & 0 & 0 & 1 \end{bmatrix} \{d_{sh,l}\}^* = [T_L]\{d_{sh,l}\}^* \tag{5}$$

where $\{d_{sh,l}\}^*$ is the column vector of untransformed element nodal displacements. In general, the transformation matrices like $[T_l]$ in Eq. (5), will also be used to transform the stiffness matrix and sectional forces from the element ends to the point CA for the shell elements (see Cook et al., 1989). Note that the sectional forces (which are measured per unit length) act at a different radial position when they are transformed. This is accounted for by a correction factor r/r_p (see Fig. 1).

Thermal Load. The heat input during welding is modeled as a thermal history, heating followed by cooling, with a simplified time and spatial variation as compared to the real welding process. The ring stiffener and the shell elements are subject to a temperature increase and decrease with maximum values at the cross-sectional area of each weld pass and a spatial variation outside the cross-sectional area of the weld pass which is estimated from the classical analytical Rosenthal solution (see, for example, Radaj, 1992). To avoid infinite temperatures at the heat source ($r = 0$ in Eq. (6)), an approximate relation will be used (Unemoto and Tanaka, 1984)

$$T(r) = T_k e^{-r/l_0}\left(\sin\left(\left(\frac{r}{l_0}\right) + \cos\left(\frac{r}{l_0}\right)\right)\right) \tag{6}$$

where $l_0 = 1.665\sqrt{k\tau}$ and k is thermal diffusion coefficient and τ is the time spent after passing a certain cross section of the pipe. The temperature T_k is here chosen as 600°C. The distance r is measured from the center point of the quadratic weld pass area $t_w \times t_w$; see Fig. 1. Note that, following the Rosenthal solutions, different spatial temperature variations were assumed for the heating and cooling step. The spatial temperature gradients are thus considerably steeper for the heating phase. In the present analysis, both the heating and cooling phases are modeled by one load step. The particular choice of times τ results in zero temperatures in the ring at roughly the radial distance $4 \times t_w$ from the center of the weld pass. As for the shell elements, their lengths were chosen to be the extent of the yield zone introduced in Moshaiov and Song (1991). This means that the length of each (left and right) shell element is $\frac{1}{3}$ of the total (half) length of the pipe. It is only these parts of the pipe that experience a change in temperature during the analysis.

The appearance of the model proposed is similar to the simplified approach proposed for the analysis of a multipass butt-welded pipe by Josefson and Karlsson (1989). There the spatial temperature variation is also obtained from the Rosenthal solution (and the temporal temperature variation is modeled very rudimentary), but the stiffness and elasto-plastic behavior of the ring and pipe is modeled by use of axisymmetric finite elements.

Numerical Algorithm. The nonlinear problem of finding the nodal degrees of freedom $\{D\}$ when the ring stiffener and the shell elements may become elasto-plastic is solved by establishing force equilibrium at the end of each load step. With no other (external) load than the temperature field, this means for the time step between t and $t + \Delta t$ that $\{F\}_{t+\Delta t} = \{0\}$. We linearize the nodal force $\{F\}$, whose components are consistent with the stress field, around a trial state $\{D\}_{t+\Delta t}^{(i-1)}$ and obtain the following system of equations, according to the Newton-Raphson approach (e.g., see Cook et al., 1989):

$$[K]_{t+\Delta t}^{(i-1)}\{\Delta D\}^{(i)} = -\{F\}^{(i-1)} = -\{F_r\}_{t+\Delta t}^{(i-1)} - \sum_{sh}\int_V B^T\{\sigma\}_{t+\Delta t}^{(i-1)}dV - [k_p]\{D\}_{t+\Delta t}^{(i-1)}$$

$$\{D\}_{t+\Delta t}^{(i)} = \{D\}_{t+\Delta t}^{(i-1)} + \{\Delta D\}^{(i)} \tag{7}$$

Here, the nodal forces for the ring $\{F_r\}_{t+\Delta t}^{(i-1)}$ are obtained from Eq. (3) and $[k_p]$ is the stiffnesses from the remote parts of the pipe. To save computer time, the elastic stiffness matrix $[k_{sh}]$ from the beginning of each load step is used for the shell elements, while the stiffness matrix $[k_r]$ is updated in each equilibrium iteration.

$$[K]_{t+\Delta t}^{(i-1)} = [k_{p,l}] + [k_{p,r}] + [k_r]_{t+\Delta t}^{(i-1)} + [k_{sh,l}] + [k_{sh,r}] \tag{8}$$

Integrals in Eqs. (7) and (8) are solved using Gaussian quadrature with 6×10 points in the ring stiffener and 2×3 points in the shell elements. We believe that it is necessary to have so many Gaussian points in order to resolve the strong temperature gradient within the ring stiffener and shell elements and also the thickness variation of the axial stress in the shell elements. However, too many Gaussian points in the shell elements may lead to plastic locking. The calculation procedure for one load step from time t to time $t + \Delta t$ can be summarized as:

1 Compute the stiffness matrix $[K]_{t+\Delta t}^{(i-1)}$. Calculate the actual temperature field in the ring and shell elements. Calculate the initial estimate $\{D\}_{t+\Delta t}^{(1)}$ from Eq. (7) with the stress $\{\sigma\}^{(0)}$ taken as the converged value from the previous load step + the stress in the ring and shell elements corresponding to the thermal strain change $\Delta\epsilon^T$ in the present load step.

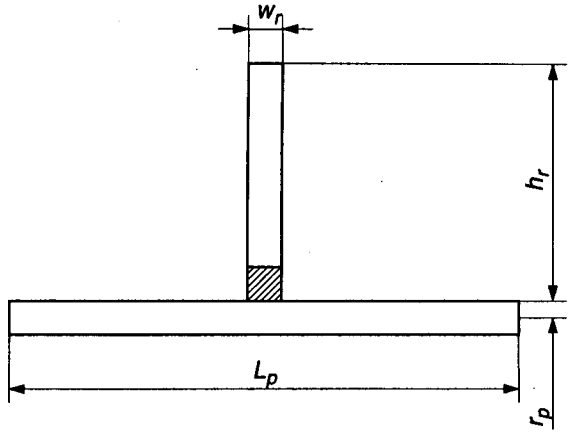

Fig. 3 Example 1: welding of ring stiffener to short pipe. One weld pass is used to simulate welding operation.

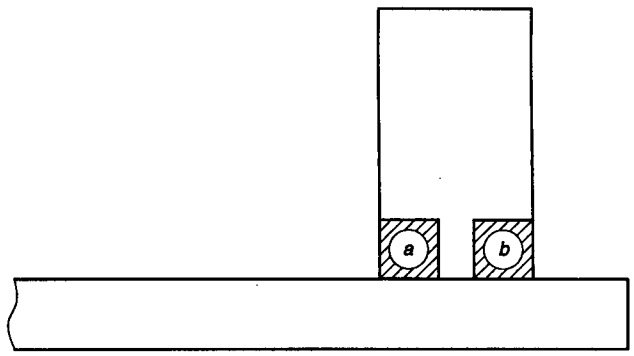

Fig. 4 Example 2: welding of ring stiffener close to end of pipe. Two weld passes are used.

2 Calculate the first estimate of the total strain at the end of the load step. For the shell elements, one obtains $\{\epsilon\}^{(i)}_{t+\Delta t} = [B]\ \{d\}^{(i)}_{t+\Delta t}$, where $[B]$ is given in Tessler (1982). For the ring stiffener, the strain is obtained from Eq. (1).

3 Update stresses in the integration points. For the ring stiffener, one first checks $|\tilde{\sigma}_{t+\Delta t} - \alpha| < \sigma_y$ where the trial stress $\tilde{\sigma}_{t+\Delta t}$ is $|\tilde{\sigma}_{t+\Delta t} = \sigma_t + E\Delta\epsilon - E\Delta\epsilon^T$. $\Delta\epsilon$ is the increment in total strain during the load step. If *yes* then the stress in this point is $\sigma_{t+\Delta t} = \tilde{\sigma}_{t+\Delta t} = \sigma_t + E\Delta\epsilon - E\Delta\epsilon^T$. If *no,* the plastic strain increment $\Delta\epsilon^p$ is calculated using Eq. (4): $|\tilde{\sigma}_{t+\Delta t} - E\Delta\epsilon^p - \alpha_t - H\Delta\epsilon^p| = \sigma_y$. The hoop stress $\sigma_{t+\Delta t}$ and translation of yield center $\alpha_{t+\Delta t}$ is then obtained as $\sigma_{t+\Delta t} = \tilde{\sigma}_{t+\Delta t} - E\Delta\epsilon^p$ and $\alpha_{t+\Delta t} = \alpha_t + H\Delta\epsilon^p$. For the shell elements, the stresses $\{\sigma\}_{t+\Delta t}$ are calculated using the effective stress function-algorithm, as presented in Kojic and Bathe (1987), including the constraint that the normal stress in the thickness direction should be zero. For the ease of implementation and to reduce computer time, the material is taken to be elastic-ideally plastic. This assumption is justified for the stainless steel studied here, since this material has a very low tangent modulus.

4 Calculate nodal forces that are consistent with the stress field in the ring stiffener and the shell elements, $\{\sigma\}_{t+\Delta t}$. For the ring stiffener, Eq. (3) is employed. For the shell elements, resultant sectional forces are first calculated (at axial locations corresponding to Gaussian points), with a result similar to Eq. (4), but including also a resultant axial and hoop normal force and a shear force. Denoting the resultant sectional forces $\{\hat{\sigma}\}^{(i)}_{t+\Delta t}$, one obtains the corresponding nodal forces as $\{F\}^{(i)}_{t+\Delta t} = \int_V [B]^T \{\hat{\sigma}\}^{(i)}_{t+\Delta t} dV$, where the strain matrix $[B]$ is taken from Tessler (1982).

5 Calculate new force unbalance (right-hand side) in Eq. (7).

6 Check for convergence in equilibrium iterations. Here, convergence is assumed to be reached when $\{\Delta D\}^{(i)^T}\{F\}^{(i-1)}_{t+\Delta t} < \delta_E\{\Delta D\}^{(1)^T}\{F\}^{(0)}_{t+\Delta t}$ where δ_E is a preset internal energy tolerance. Here, we have used $\delta_E = 1 \times 10^{-3}$. If *yes,* return to point 1 for the next load step. If *no,* return to point 2 for a new equilibrium iteration within this load step.

Numerical Examples. The method proposed in the foregoing will be used to calculate welding residual deformations in three examples. Temperature-dependent values for the stainless steel material is taken from handbooks. Thus, the room temperature values for the material parameters are: Young's modulus $E = 210$ GPa, Poisson's ratio $\nu = 0.3$, virgin yield stress $\sigma_Y = 220$ MPa, tangent modulus $E_t = 2.1$ GPa, and the linear thermal expansion coefficient $\alpha_T = 1.6 \times 10^{-5}°C^{-1}$.

Example 1. In the first example, the welding of a ring to a short thin-walled pipe is studied. The ring is placed symmetrically on the pipe. This problem was studied in Moshaiov and Song (1991) using a semi-analytical single-degree-of-freedom (1-dof) method. The residual radial displacement was calculated for several combinations of geometrical parameters for the pipe ring assembly. The 1-dof method is partly calibrated against detailed FE-analyses, also reported in Moshaiov and Song (1991). Hence, the agreement between semi-analytical and FE-results is very good. Unfortunately, there is no information in Song and Moshaiov (1990) on the weld geometry and weld parameters used. We have assumed one weld pass with quadratic cross section with the area $w_r \times t_w$, where $t_w = 6.35$ mm; see Fig. 3. The ring stiffener and pipe thickness w_r and t_p had the constant value 6.35 mm in the analysis. Table 1 shows calculated residual radial displacement of the ring using our approach (w) together with results from the FE-simulations (labeled 3a, 3b, and 3a6) referred to in Moshaiov and Song (1991). The FE-results are denoted w_{Ref} in the table. The total length of the cylinder is $L_p = L_l + w_r + L_r$.

One finds that our approach gives qualitatively the same result as the FE-results from Moshaiov and Song (1991). One may note that the material in the FE-calculations in Moshaiov and Song (1991) is a "mild steel," which will probably have a higher yield strength than stainless steel. This will slightly increase the inward residual radial displacement.

Example 2. In the second example two-pass fillet welding of a ring close to the end of a pipe is studied; see Fig. 4. Hence, one should anticipate that there will be a rotation of the ring. The ring and pipe have the following dimensions: pipe mean radius, $r_p = 82.5$ mm, pipe length, $L_p = 150$ mm, pipe wall thickness, $t_p = 5.0$ mm, ring height, $h_r = 20$ mm, and ring thickness, $w_r = 10$ mm. The weld passes are assumed to have a quadratic shape with the side $t_w = 4$ mm. Table 2 shows the

Table 1 Calculated residual radial ring displacement, w, for pipe with symmetrically placed ring stiffener. Influence of different geometrical parameters.

Case	r_p [mm]	L_p [mm]	h_r [mm]	w [mm]	w_{Ref} [mm]
3a	447	76.2	50.8	−0.25	−0.3
3c	447	50.8	21.5	−0.61	−0.54
3a6	1447	76.2	50.8	−0.80	−0.71

Table 2 Calculated residual radial displacement, w, and cross section rotation, θ, for pipe with ring stiffener located close to one end. Influence of weld sequence.

Sequence	w [mm]	θ [deg]
a before b	−0.21	−0.40
b before a	−0.15	0.37

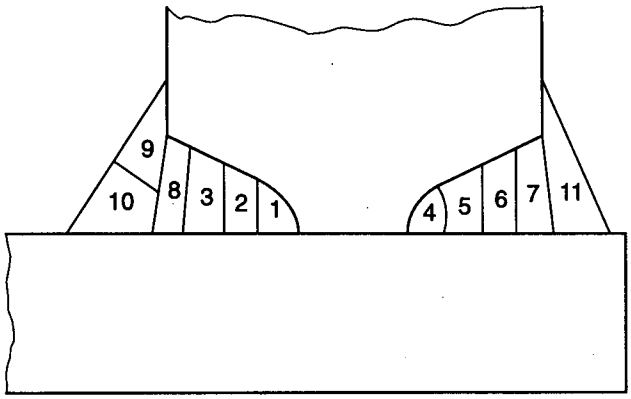

Fig. 5 Cross section of double-J eleven pass butt-weld. The numbers show welding sequence used. (From Troive and Jonsson, 1994.)

residual radial deflection and rotation of the ring for the two cases: 1) pass a is welded before b; and 2) pass b is welded before a.

Example 3. In the final example, the multipass welding of a ring stiffener to the end of a pipe is studied. For this geometry, both experimental results and calculated results from a detailed FE-analysis are available (Troive and Jonsson, 1994). The numerical analysis included nonlinear thermal and subsequent mechanical FE-analyses. The pipe has a inner radius of $r_p = 84$ mm, a wall thickness of $t_w = 8$ mm, and the total length is $L_p = 200$ mm. The ring stiffener has an outer radius of 134 mm and the thickness $w_r = 22$ mm. Both the pipe and ring stiffener are made of stainless steel. Figure 1 shows the lay-out of the pipe ring stiffener assembly. The weld joint was made up of eleven passes using manual arc welding. The welding sequence is displayed in Fig. 5. An average value (around the circumference) for the radial displacement and cross-sectional rotation of the ring was experimentally found to be −0.75 mm and 2.3 deg, respectively. These results were obtained by careful measuring on the welded pipe. The corresponding calculated values from the detailed FE-analysis in Troive and Jonsson (1994) were −1.2 mm and 1.5 deg. The calculated results with our present approach were −0.8 mm and 1.1 deg, respectively. Hence, the present approach gives qualitatively correct results, but the solution is somewhat stiff. One source of uncertainty is the accumulated bulk temperature increase in the pipe due to the large number of weld passes. This effect is not considered in our simplified analysis. For manual arc welding, this bulk temperature increase may be substantial. In our simplified approach, one finds normally that, for example, a weld pass deposited on the left side of the ring stiffener (Fig. 1, or to the left of the ring stiffener in Fig. 5) will give a positive (counterclockwise) cross-sectional rotation. However, this may not be the case when the stiffener is located close to one end. Therefore, it is difficult to predict, beforehand, the sign of the residual cross-sectional rotation of the ring; see, also, the Discussion. This example can also be used to compare the CPU-time needed for the computations. The detailed FE-analysis (Troive and Jonsson, 1994) took 12 h on a SUN Sparc-10 workstation (using an in-house FE-code), while the present analysis (coded in MATLAB) took roughly 2 min on the same workstation.

Discussion

The present approach seems to be a good compromise between a reasonable accuracy in the prediction of welding residual displacements and the need for low computer times. With this approach, it is possible to reproduce experimental results from the literature for single-pass welds (Moshaiov and Song, 1991) and multipass welds (Troive and Jonsson, 1994) without performing a detailed thermal and mechanical FE-analysis.

There exist of course even simpler analytical models, where the pipe and the ring stiffener are elastic and where the ring stiffener is subject to a temperature decrease in the area of each weld pass (see Bushnell, 1976). First, one may model the ring stiffener as in the foregoing, and the pipe solely as a thin-walled pipe subject to sectional forces at one end and with no temperature load. Secondly, one may improve this model by introducing a temperature load in the pipe. This is most conveniently achieved by dividing each pipe part into one shell finite element and one remote part subject only to end forces. These two elastic models are much faster than the present approach. However, with the material being elastic, they will give too small residual displacements since they tend to be too stiff.

We have found that it is essential to include plastic deformations in the ring and temperature increases and decreases, as well as plastic deformation in parts of the pipe located closest to the ring stiffener. However, since the stress state in a thin-walled pipe is biaxial, it is more difficult to describe plastic deformation in the pipe than in the ring. More degrees of freedom are needed, which increases the computational time. It is believed that the most rational way to include plasticity and thermal loading in parts of the pipe is to divide the pipe halves into one shell element and one part which is always elastic and at room temperature. One final remark is that the most important factor for accurate predictions of residual deformations is the shape of the temperature field. For the case of welding a ring stiffener to a pipe, this means that the extent of the heated zone to large parts of the ring and pipe halves must be modeled if accurate residual displacements is desired.

The experimental investigation of the pipe ring assembly reported in Troive and Jonsson (1994) revealed some drawbacks of the present semi-analytical approach:

- Rotational symmetry often does not prevail, particularly for cases when manual arc welding is employed, resulting in low welding speeds.
- The cross-sectional area of the ring may deform noticeably, which means that the stress state in the ring is not purely uniaxial.
- During welding the ring stiffener may not be "rigidly" connected to the pipe. This will probably often be the case during the first passes of a multipass welding. The ring stiffener is then very weak close to the outer surface of the pipe due to the groove preparation. Indeed, a noticeable difference between ring stiffener and pipe deformations was observed during the first passes.

References

Barborak, D. M., Dickinson, D. W., and Madigan, R. B., 1991, "PC-Based Expert Systems and Their Application to Welding," *Welding Journal,* Vol. 70, pp. 29–38.

Brown, S. B., and Song, H., 1992, "Implications of Three-Dimensional Numerical Simulations of Welding Large Structures," *Welding Journal,* Vol. 71, pp. 55s–62s.

Bushnell, D., 1976, "BOSOR5-Program for Buckling of Elasto-Plastic Complex Shells of Revolution Including Large Deflections and Creep," *Computers & Structures,* Vol. 6, pp. 221–240.

Chen, B., and Peng, J., 1994, "Expert Systems and Their Development," *Welding in the World,* Vol. 34, pp. 247–253.

Cook, R. D., Malkus, D. S., and Plesha, M. E., 1989, *Concepts and Applications of Finite Element Analysis,* Third Edition, John Wiley & Sons, New York, NY.

Goldak, J., Oddy, A., Gu, M., Ma, W., Mashaie, A., and Hughes, E., 1992, "Coupling Heat Transfer, Microstructure Evolution and Thermal Stress Analysis in Weld Mechanics," *Mechanical Effects of Welding* IUTAM-Symposium, Luleå Sweden, eds, L. Karlsson, L.-E. Lindgren, and M. Jonsson, Springer-Verlag, Berlin, Germany, pp. 277–287.

Josefson, B. L., and Karlsson, C. T., 1989, "FE-Calculated Stresses in a Multi-Pass Butt-Welded Pipe—A Simplified Approach," *International Journal of Pressure Vessels and Piping,* Vol. 38, pp. 227–243.

Josefson, B. L., 1993, "Prediction of Residual Stresses and Distortions in Welded Structures," ASME JOURNAL OF OFFSHORE MECHANICS AND ARCTIC ENGINEERING, Vol. 115, pp. 52–57.

Kojic, M., and Bathe, K.-J., 1987, "Thermo-Elastic-Plastic and Creep Analysis of Shell Structures," *Computers & Structures,* Vol. 26, pp. 135–143.

Lucas, W., 1994, "Experiences in Developing Expert Systems and Neural Networks for Arc Welding," *Welding in the World,* Vol. 34, pp. 237–245.

Moshaiov, A., and Song, H., 1990, "Near- and Far-Field Approximation for Analyzing Heating and Welding," *Journal of Thermal Stresses,* Vol. 13, pp. 1–19.

Moshaiov, A., and Song, H., 1991, "Modeling of Welding Distortion in Stiffened Rings," *Journal of Ship Research,* Vol. 35, pp. 162–171.

Radaj, D., 1992, *Heat Effects of Welding,* Springer-Verlag, Berlin, Germany.

Song, H., and Moshaiov, A., 1990, "Modeling of Distortion in Girth-Welded Thin Pipes," ASME *Journal of Pressure Vessel Technology,* Vol. 112, pp. 266–272.

Tessler, A., 1982, "An Efficient, Conforming Axisymmetric Shell Element Including Transverse Shear and Rotary Inertia," *Computers & Structures,* Vol. 15, pp. 567–574.

Troive, L., and Jonsson, M., 1994, "Numerical and Experimental Study of Residual Deformations due to Double-J Multi-Pass Butt-Welding of a Pipe-Flange Joint," *Proceedings of the IEMS 94* (1994 Annual International Conference on Industry, Engineering and Management Systems), Cocoa Beach, FL.

Unemoto, T., and Tanaka, S., 1984, "A Simplified Approach to Calculate Weld Residual Stresses in a Pipe," *IHI Engineering Review,* Vol. 17, pp. 177–183.